Design optimization of a compact photonic crystal microcavity based on slow light and dispersion engineering for the miniaturization of integrated mode-locked lasers

Malik Kemiche, Jérémy Lhuillier, Ségolène Callard, and Christelle Monat

Citation: AIP Advances **8**, 015211 (2018); doi: 10.1063/1.5008476
View online: https://doi.org/10.1063/1.5008476
View Table of Contents: http://aip.scitation.org/toc/adv/8/1
Published by the American Institute of Physics

Design optimization of a compact photonic crystal microcavity based on slow light and dispersion engineering for the miniaturization of integrated mode-locked lasers

Malik Kemiche,[a] Jérémy Lhuillier, Ségolène Callard, and Christelle Monat
Université de Lyon, Institut des Nanotechnologies de Lyon (INL) UMR 5270, École Centrale de Lyon, 69134 Écully, France

(Received 6 October 2017; accepted 28 December 2017; published online 10 January 2018)

We exploit slow light (high n_g) modes in planar photonic crystals in order to design a compact cavity, which provides an attractive path towards the miniaturization of near-infrared integrated fast pulsed lasers. By applying dispersion engineering techniques, we can design structures with a low dispersion, as needed by mode-locking operation. Our basic InP SiO_2 heterostructure is robust and well suited to integrated laser applications. We show that an optimized 30 μm long cavity design yields 9 frequency-equidistant modes with a *FSR* of 178 *GHz* within a 11.5 *nm* bandwidth, which could potentially sustain the generation of optical pulses shorter than 700 *fs*. In addition, the numerically calculated quality factors of these modes are all above 10,000, making them suitable for reaching laser operation. Thanks to the use of a high group index (28), this cavity design is almost one order of magnitude shorter than standard rib-waveguide based mode-locked lasers. The use of slow light modes in planar photonic crystal based cavities thus relaxes the usual constraints that tightly link the device size and the quality (peak power, repetition rate) of the pulsed laser signal. https://doi.org/10.1063/1.5008476

I. INTRODUCTION

Periodic trains of short optical pulses delivered by mode-locked lasers in the near infra-red are of particular importance for a wide range of applications including high speed optical communications,[1] clock recovery,[2] optical sampling[3] and even bio-mimetic systems.[4] While there have been a number of approaches for realizing mode-locked lasers, most of the systems developed thus far consist of relatively bulky and stand-alone laser devices made of either free-space, fiber optics or semiconductor optical components. There has been some progress towards the miniaturization of these devices,[1,5–14] in particular for semiconductor pulsed lasers,[1,5–12] but their dimensions remain typically in the millimeter to centimeter range. The size of these stand-alone components is still too high for some of the aforementioned applications, where source integration could also bring real advantages in terms of robustness, stability and throughput. In parallel to the development of silicon photonics and the efforts for integrating on the same chip-based platform various optical building blocks, such as low loss waveguides, modulators, multiplexers, photo-detectors and light sources, the integration of compact devices emitting a train of short optical pulses on-chip remains elusive.

The hybrid integration of III-V and silicon materials[15–19] has provided a critical step towards the development of integrated continuous-wave lasers on a silicon chip. Combined with compact optical resonators, such as micro-disks[16,17] and planar photonic crystal (PhC) based cavities,[19–22] these approaches have resulted in the integration of miniaturized light sources that can directly feed laser

[a]Electronic mail: malik.kemiche@doctorant.ec-lyon.fr

light into a silicon photonic integrated circuit underneath.[17–22] Though direct modulation of these lasers is possible, they can hardly produce optical pulses that are shorter than a few nanoseconds, with at best a few tens of GHz repetition rate.[23] The integration of faster mode-locked laser components has been demonstrated recently, which use several phase-locked frequency-equidistant modes, but the underlying cavity typically exploits a standard strip-based waveguide, whose length is still above 500 μm.[1,5–10,12]

In this context, exploiting nanophotonic concepts such as PhC for reducing the cavity size is key to realizing more compact pulsed laser devices. Indeed, several critical parameters of mode-locked lasers, which directly impact their performance (peak power of the pulse, short pulse duration, repetition rate...), are directly proportional to the product of the group index and the length of the cavity $n_g L$. This explains the difficulty in miniaturizing the mode-locked laser without degrading the quality of the pulsed laser signal. Besides, the reduction in the cavity size is often accompanied by an increase of the optical losses, which increase the power consumption of the laser. Controlling the group index through the use of PhC based nanophotonic concepts provides an additional degree of freedom that relaxes the tight constraints between the mode-locked laser characteristics and the size of the cavity.

We exploited here slow light (high n_g) modes in PhCs for designing a compact cavity that could provide an effective path towards the miniaturization of near-infrared integrated mode-locked lasers. Although PhC slow light modes tend to be highly dispersive, we applied dispersion engineering techniques in order to reach the low dispersion that is required for cavity mode-locking. The basic heterostructure we considered for our design consists of an active InP membrane on a silica low index substrate, which is robust and well suited to laser applications while offering the possibility for the deposition of a saturable absorber on top of it for mode-locking operation. Our optimized cavity design provides at least 9 frequency-equidistant modes with a *FSR* of 178 *GHz* within a 11.5 *nm* bandwidth, which could potentially sustain the generation of optical pulses shorter than 700 *fs*. In addition, we numerically studied the quality factors of these modes and showed that they all lie in a range (>10, 000) that makes them suitable for enabling laser operation. Most importantly, thanks to the use of a relatively high group index (28), our cavity is only 30 μm long, i.e. almost one order of magnitude shorter than standard rib-waveguide based designs of semiconductor mode-locked lasers.

II. APPROACH AND SIMULATIONS

A. Approach for the cavity design

Considering our long-term goal of realizing a compact and integrated mode-locked laser on a chip, we designed and optimized our cavity geometry so as to generate numerous frequency-equidistant modes in a short cavity (typically below 100 μm), with quality factors sufficient to sustain laser oscillations ($Q >$ sev. 1000). The number N of these modes should be high enough to achieve high peak power of the future pulsed laser, which increases with N^2. The basic heterostructure we considered in our design work consists of an active indium phosphide slab that is supported on a thick silica insulating layer, so as to enable the future integration of the laser with a silicon based photonic integrated circuit.[16,17,19,20,22] A PhC cavity based on a linear defect waveguide is inscribed in the InP slab (see Figure 1). Compared with a more traditional geometry where the slab is suspended in air,[24] this structure is mechanically more robust and improves the laser heat dissipation.[25] Besides, in contrast with a fully cladded geometry where the InP slab would be completely buried in silica, our design offers the possibility to integrate a saturable absorber on top, e.g. through a post-process mechanical transfer, so as to ensure a substantial interaction with the laser modes, as intended for mode-locking operation. However, the less efficient vertical confinement of the mode associated with the light line of silica (as opposed to air) on the one hand, and the coupling between TE/TM modes induced by the vertical asymmetry of the structure[26] on the other hand, bring additional constraints to the cavity design. In particular, they may have a non-negligible impact on the mode quality factors, which we study in the last section.

As shown in Table I, the performance of the intended mode-locked laser, e.g. the number of modes N, the pulsed laser peak power and its repetition rate directly depend on the product of the

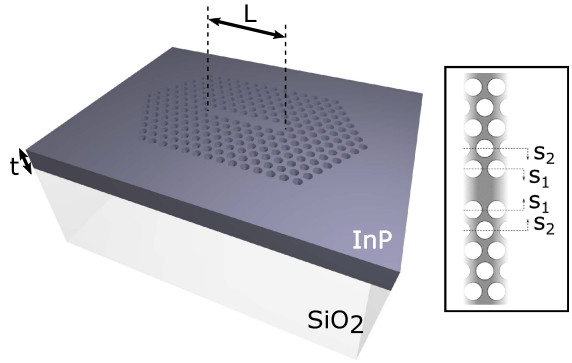

FIG. 1. Schematic of the structure. s_1 and s_2 are the parameters to be optimized to engineer the dispersion of the W1 waveguide.

group index related to the traveling mode in an elongated cavity and the length of this cavity n_gL. Indeed, n_gL represents the effective optical path length of the cavity, and thus determines the number of modes. This means that a reduction of the mode group velocity, or slow light (high n_g), can be used to counterbalance the reduction of N caused by the miniaturization of the cavity length. Our approach thus consists of exploiting slow light modes in elongated PhC based cavities. These modes are typically highly dispersive, which leads to a spectrally narrow comb of frequency-equidistant modes. Here, we adapted dispersion engineering techniques and optimized the geometry of the PhC structure to create a non-dispersive band affording high and constant n_g modes across a large bandwidth $\Delta\omega$. The underlying dispersion engineered waveguides were first optimized (section II B 1) and served as a starting point for our cavity design. We then investigated the elongated cavities created through closing both ends of these waveguides by PhC mirrors. The spectral signature of the cavity and the mode quality factors, as potentially impacted by our particular asymmetric geometry, were investigated afterwards (section II B 2).

Dispersion engineering in PhC waveguides has been extensively investigated for passive silicon structures suspended in air[27] and led to applications in nonlinear optical signal processing.[28] In this study, we chose to apply and optimize the approach developed by Li *et al.*[27] to engineer flat band slow light modes in active asymmetric InP PhC waveguides with the additional constraints mentioned above. It was shown that flat band slow light modes could be achieved in PhC waveguides by modifying the lateral position of the first two rows of holes adjacent to the line defect. This effectively modifies the coupling between the refractive and the gap guided modes so as to flatten the dispersion of the guided mode. The performance of the PhC waveguide design can be evaluated by the figure of merit (FoM) $n_g\frac{\Delta\omega}{\omega}$, where n_g is the mean group index of the linear band, ω is its mean angular frequency, and $\Delta\omega$ is the bandwidth across which the group index n_g is constant within a ± 10% margin. Both the light slow-down factor and the bandwidth of the linear band included in the FoM are critical to the performance of the mode-locked laser device (see Table I). Furthermore, we evaluated the second-order dispersion from a Taylor expansion of the flat band around its center. The optimum design is obtained by tuning the position of the first two rows of holes to achieve the highest FoM and the smallest dispersion.

TABLE I: Relations between the performance characteristics of the mode-locked laser and the parameters of the underlying elongated cavity (group index n_g, length L, and bandwidth $\Delta\omega$ of the low dispersion band). Note that $\Delta\omega$ is either limited by the cavity geometry dispersion or by the active material spectral gain variation.

Laser characteristics	Parameters
Number of modes	$N \propto n_gL \times \Delta\omega$
Peak power	$P_{peak} \propto N^2 \propto (n_gL \times \Delta\omega)^2$
Repetition rate	$f_{rep} = FSR = c/(2 \times n_gL)$
Pulse duration	$\Delta t_{pulse} \geq 2\pi/\Delta\omega$

In our simulations, we used a triangular lattice of cylindrical air holes (period $a = 414nm$, hole radius $r = 118nm = 0.286a$) patterned in an InP slab of thickness $t = 300nm$ and refractive index 3.167 around a wavelength of 1.55 μm bonded onto a thick SiO_2 substrate of index 1.444 (considered vertically infinite in the calculations). The PhC is designed so as to present a TE (**E** ∥ InP slab) photonic band gap around 1.55 μm. The so-called W1 waveguide is formed from one missing row of holes along the ΓK direction of the PhC lattice and surrounded by 11 rows of holes on both sides, which are sufficient to ensure a good lateral confinement of the optical mode. The shifts of the first and second rows towards the central axis of the waveguide are denoted by s_1 and s_2 respectively. Figure 1 shows a schematic of the structure with all geometric parameters labeled.

B. Simulation results

1. Guided mode dispersion

First, a W1 waveguide was studied using the 2D Plane Wave Expansion (PWE) method and the effective index approximation to identify the values of s_1 and s_2 that maximize the FoM. Figure 2 shows the evolution of the FoM $n_g \frac{\Delta\omega}{\omega}$ and n_g with respect to s_1 and s_2. These results showed that several pairs of (s_1,s_2) could maximize the FoM (around 0.3). They are located in a valley where s_2 can be chosen to adjust n_g (displayed as contour lines on Figure 2). Based on these guidelines, three configurations were studied, which should provide roughly similar FoMs (close to the maximum) but three different values of n_g varying between 10 and 20. Note that whilst 2D PWE simulations quickly yielded the trend for the evolution of the FoM according to the design parameters, they are not fully reliable and underestimate, in particular, the value of n_g. Using these preliminary results, we switched to 3D FDTD.

Lumerical 3D FDTD allows us to account for the vertical asymmetry of the structure, as well as for the dispersion of all materials (InP and silica), which are embedded in the software. Following the 2D PWE results, three values of s_2 were studied ($-0.1a$, $0a$ and $0.036a$, i.e. -42 nm, 0 and 15 nm) to reach various group indices, and for each of them, the optimal value of s_1 was found by 3D FDTD simulations. Figure 3(a) presents the group indices of 6 structures with s_1 varying from $-0.135a$ to $-0.115a$ while s_2 is kept equal to 0. To evaluate the band flatness, the mode second-order dispersion $\beta_2 = \frac{d^2k}{d\omega^2}$ was calculated for each structure by fitting the flat band with a third-order polynomial.

Figure 3(b) shows the evolution of both the FoM and β_2 (in ps^2/km) with respect to s_1. The highest FoM is achieved for $s_1 = -56nm$ ($0.136a$), with $n_g \frac{\Delta\omega}{\omega} = 0.295$. Note that this is close to the maximum that can be obtained in the silicon-air structure.[27] The optimum value of s_1 actually results from a trade-off between the flat band slow light bandwidth and the high-order dispersion, as illustrated on the different curves of Figure 3(b). Theoretical studies of the dynamics in mode-locked lasers showed that β_2 values between -1 and -4×10^6 ps^2/km were low enough to sustain mode-locking operation.[29] By taking into account this last criterion, the highest FoM is achieved for $s_1 = -53$ nm.

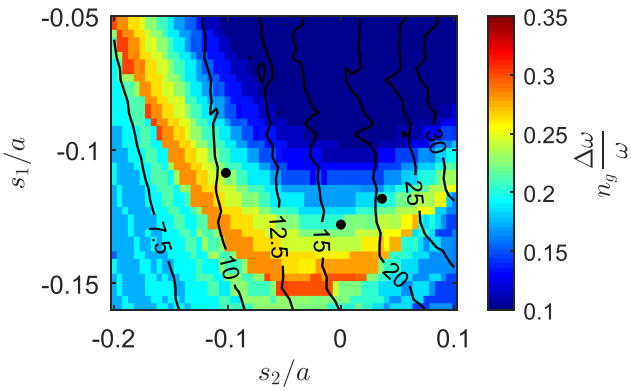

FIG. 2. Figure of merit map with respect to s_1 and s_2 obtained from 2D PWE simulations on engineered W1 PhC waveguides. Contour lines represent constant n_g values. The black dots highlight the (s_1,s_2) designs that were eventually chosen according to 3D FDTD simulations.

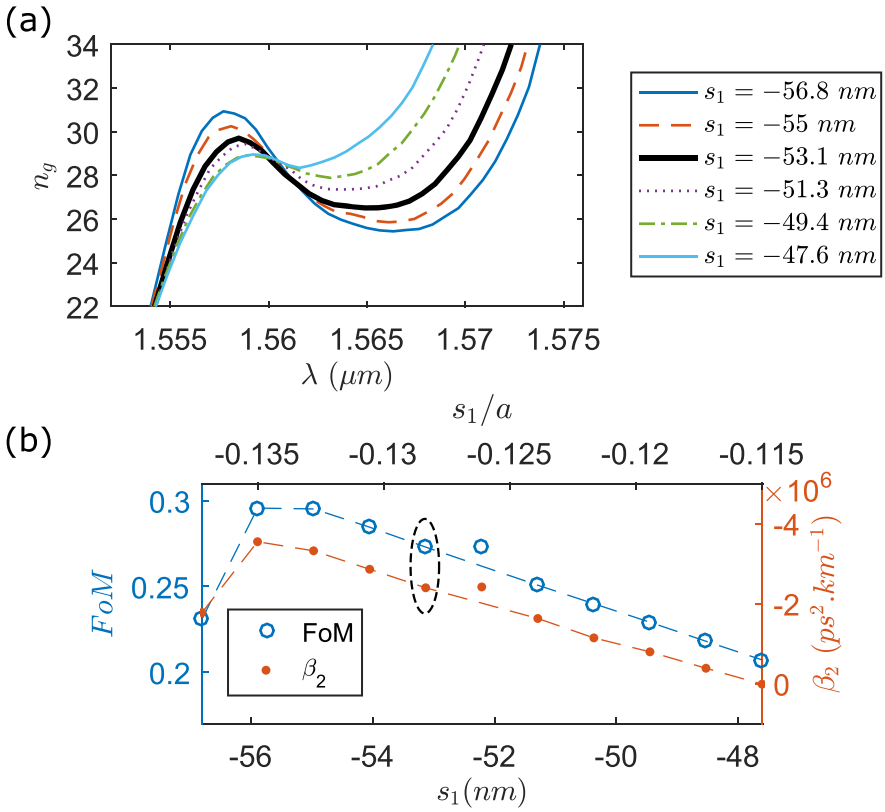

FIG. 3. (a) Group index spectral variation of the modified W1 waveguide fundamental TE mode calculated by 3D FDTD for $s_2 = 0$ and s_1 varying from $-57nm$ ($0.138a$) to $-47.6nm$ ($0.115a$). The chosen trade-off is highlighted by the solid black line. (b) Evolution of the $FoM = n_g \frac{\Delta\omega}{\omega}$ and the second-order dispersion β_2 with respect to s_1. The chosen design is circled in black.

Similar numerical studies were carried out for the other values of s_2, resulting in three optimized geometries with $n_g = 16$, $n_g = 28$ and $n_g = 40$ (see Table II for a summary of their characteristics). Figure 4 shows the three associated mode dispersions and the spectral dependence of the related group index. Note that the central wavelengths of the flat band slow light are slightly blueshifted for increasing n_g (i.e. s_2) but this could be readily compensated for by adjusting the PhC geometric parameters (period, filling factor). As expected, increasing the group index leads to a narrower $\Delta\omega$, since the FoM is almost unchanged. These various optimized designs could be chosen alternatively depending on the intended application, and how critically size reduction of the laser is needed. While the light line of air falls outside the spectral window represented in Figure 4(a), the light line of silica, which governs the vertical confinement of the modes in our PhC structures, crosses the optimized flat band slow light, highlighting the additional challenges associated with the laser heterostructure under study as compared with PhC membranes suspended in air. This could potentially reduce the quality factors of the associated cavity modes, thereby effectively decreasing the number of modes to be exploited for mode-locking operation. Note that the 300 *nm* slab thickness was precisely chosen so as to increase the bandwidth of the flat band slow light under the silica light line. We investigate

TABLE II. Summary of the three designs obtained by 3D FDTD simulations of dispersion-engineered W1 waveguides.

n_g	$s_1\ (nm)$	$s_2\ (nm)$	$n_g \frac{\Delta\omega}{\omega}$	$\beta_2\ (ps^2.km^{-1})$
16	-45	-42	0.296	-1.74×10^6
28	-53	0	0.273	-2.4×10^6
40	-49	15	0.261	-5.6×10^6

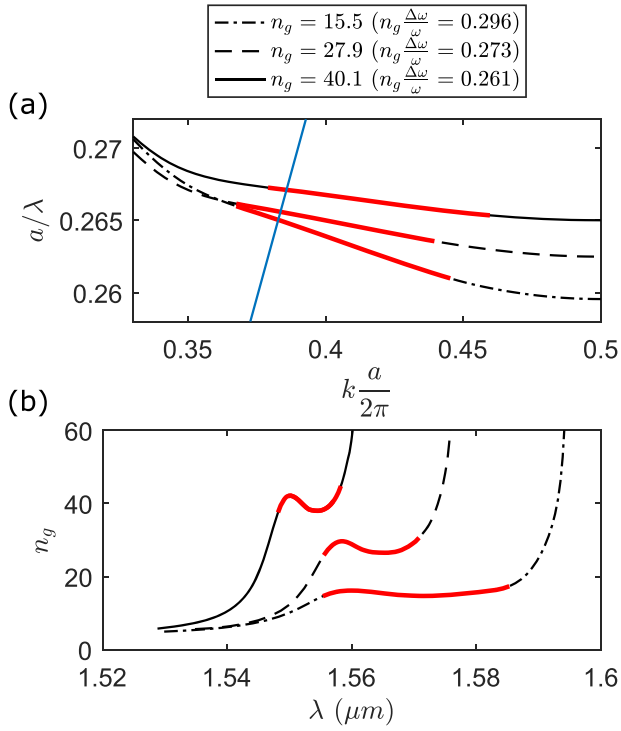

FIG. 4: 3D FDTD simulated (a) dispersion and (b) group index of the TE fundamental mode associated with the three optimized PhC waveguide geometries yielding $n_g = 16$, $n_g = 28$ and $n_g = 40$. The flat band slow light is highlighted by the red thick solid line. The blue line represents the light line of silica.

the optical losses associated with these cavity modes in the next section so as to clarify whether they are high enough for enabling laser operation.

2. Cavity simulations

The optimized waveguide designs were used as a starting point to create linear defect PhC cavities (Figure 1) by adding PhC mirrors at both ends of the waveguide. We first verified that the spectral signature of the cavity exhibits the intended regular comb of modes, as expected from the linear waveguide dispersion. We then calculated, by 3D FDTD simulations, the quality factor of these modes, a critical specification for sustaining laser operation. As an illustration example, we studied a cavity of length $L = 30\mu m$, associated with a line defect of 73 missing holes based on the $n_g = 28$ waveguide design ($s_1 = -53$ *nm*, $s_2 = 0$). To draw a comparison with the guided mode dispersion, the cavity mode frequencies are plotted against k values equal to integer increments of π/L and superimposed on the dispersion curve of the simulated W1 waveguide on Figure 5. We find 9 equally-spaced modes in the flat band slow light window below the light line, spanning across a bandwidth of 11.5 *nm* (1.42 *THz*), potentially yielding 0.7 *ps* pulse duration upon mode-locking of these modes. This bandwidth is slightly lower than that of the flat band (1.88 *THz*), since modes above the light line were a priori ruled out. A linear regression on these mode frequencies gives a free spectral range around 178 *GHz* and a correlation coefficient of 0.9995. According to the relation from Table I, $FSR = \frac{c}{2n_g L}$, this *FSR* actually corresponds to a cavity with $n_g = 28$, i.e. a value consistent with the waveguide simulations (Table II).

Figure 5 also displays the quality factors of these 9 modes, which are all above 10,000. We note that this value should be high enough for sustaining laser emission, even considering the typical degradation (up to a factor of 10) of the Q factor arising upon fabrication with standard lithography/etching processes. The effect of the silica light line, which provides an additional optical loss channel in the silica substrate, can clearly be seen as the mode quality factors drop from values over 10, 000 to ≈ 1000 upon increasing mode frequencies and eventually crossing the light line. However,

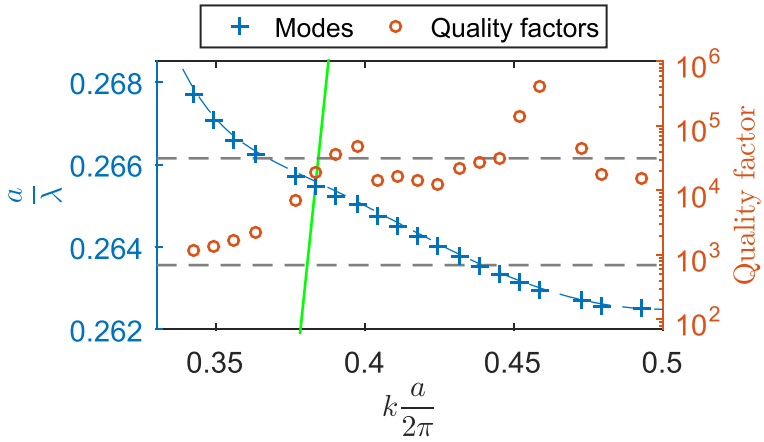

FIG. 5. Modes of the L73 cavity obtained by 3D FDTD calculation (blue crosses) and their quality factor (red circles). The dashed blue line represents the fundamental mode dispersion of the related optimized W1 waveguide. The limits of the flat band slow light are shown as gray dashed lines.

we note that some modes just above the light line and within the flat band slow light do exhibit a quality factor close to 10, 000, which is still high enough for our laser mode-locking application. So, the aforementioned values of 9 modes and 11.5 *nm* for the related bandwidth are slightly underestimated, since a few more modes could easily take part in mode-locking operation, especially in longer cavities. Finally, this 10,000 Q-factor value is relatively low with respect to the values that can be achieved in PhC cavities. The study presented in the next section aims at identifying the main contributions to these optical losses.

III. DISCUSSION AND RESULTS

Our simulations assess the validity of the slow light PhC approach explored in a practical configuration (InP membrane on a low index substrate) for yielding a comb of modes with sufficiently low optical losses and a regular spectral spacing so as to sustain mode-locked laser operation with suitable characteristics. Now, considering the non-negligible optical losses ($Q \approx 10,000$) experienced by these PhC cavity modes, we analyze their physical origins.

Standard models for the optical losses in elongated cavities distinguish the contributions of distributed losses and losses caused by the imperfect mirrors at both ends of the cavity. To clarify their relative weight in our structures, we performed 3D FDTD simulations on PhC cavities with different lengths. The mean quality factor of the modes lying in the flat band (under the light line) is plotted on Figure 6 with respect to the cavity length L. The numerical results were fitted by a classical loss model for Fabry-Pérot cavities (dashed line on Figure 6), which considers that the effective total loss per meter is given by $\alpha_{eff} = \alpha_d - 1/Lln(R)$, where R is the reflectivity of the mirrors at the cavity ends (assumed to be constant for all modes) and α_d (in m^{-1}) is the distributed loss along the cavity. As expected, the mirror losses and the distributed losses alternately dominate for short and long cavities, respectively. There is some discrepancy with this simple model for short cavities ($L < 4\ \mu m$), which yield only one cavity mode in the flat band, whose out-of-plane losses at the mirrors may vary with its spectral distance from the light line. However, since the value of α_{eff} is more relevant for multimode cavities, as intended for mode-locking operation, the fit was done by ignoring the Q points associated with short cavity lengths, where the number of modes is less than 2. For cavities with L above 10 μm, the mirror loss becomes negligible and the total Q-factor saturates to about 20,000, dominated by the distributed loss α_d. Since the long cavity modes are situated below the light line and the number of PhC rows at either sides of the waveguide defect is high enough to block optical losses in the plane, the propagation loss α_d should primarily be caused by the structure asymmetry.[26] Indeed, the latter enables the excited TE modes to couple to TM modes, for which there is no photonic band gap in this range of frequencies. To evaluate this additional loss channel, we performed 3D FDTD

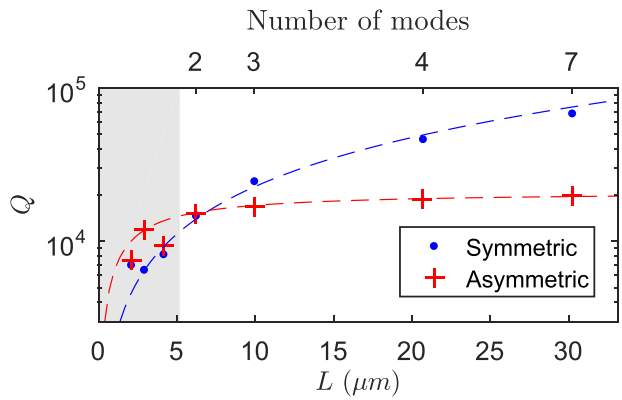

FIG. 6: Evolution of the mean quality factor Q of linear defect cavities, as calculated by 3D FDTD for the asymmetric (red dots) and symmetric (blue dots) configurations. The dashed lines show the fits according to the model $\alpha_{eff} = \alpha_d - 1/Lln(R)$. The number of modes taken into account for the estimation of the Q (i.e. within the flat band slow light and below the light line) for each cavity length is shown on the top x axis. The gray area represents the cases where only one mode can be found in the flat band.

simulations for symmetric PhC cavities with the same geometry (air holes in InP) but surrounded by silica below and above. We evaluate the mean quality factor for the cavity modes within the flat band and plot it against the cavity length in Figure 6. The values of R and α_d used for fitting the Q-factors using the linear regressions provided by the standard loss model are presented on Table III. The comparison between the two geometries shows first that the mirror reflectivity is slightly better in the asymmetric structure, probably due to a better light confinement of the modes inside the slab provided by the air/InP interface at the top. This results in higher Q-factor cavity modes for short asymmetric cavities with respect to their symmetric counterparts. Most importantly, however, the distributed losses are one order of magnitude lower for the symmetric case with respect to the asymmetric one, confirming the predominant role of the TE/TM coupling in the loss mechanism for long asymmetric cavities. This 10 times larger distributed loss leads to a reduction of the Q-factor for long cavities from 100,000 to 20,000. Although the structure vertical asymmetry thus limits the Q-factor of elongated cavity modes to about 20, 000, it provides access to the top of the structure, enabling us to integrate a saturable absorber for mode-locking operation, or to carry out near-field observations. If needed though, it is possible to make the structure symmetric to increase the quality factors, but we reemphasize that their value should already be high enough to observe stimulated emission.

Regarding the number of modes involved in mode-locking operation, examples of integrated mode-locked lasers[9,10] show that tens of modes are sufficient to achieve pulsed light signals with high quality to be exploited in applications, for instance for high data rate transmission.[1] In the 30 μm long PhC cavity presented above, there are 9 or 10 modes susceptible to take part in mode-locking operation. Since the number of modes is proportional to the cavity length (see Table I), it can be increased through simply using a longer cavity. With a 100 μm long cavity, for example, there should be at least 30 modes in the flat band slow light. In addition, the bandwidth of the flat band slow light (around 10nm) is compatible with the generation of sub-picosecond short optical pulses ($\approx$700fs in duration) and corresponds to the typical values used in semiconductor mode-locked lasers. Indeed, in these devices, the spectral band where the gain of the active material is flat

TABLE III. Fit parameters of the loss model from 3D FDTD simulations for both symmetric elongated cavities and asymmetric ones.

Structure	α_d ($dB.mm^{-1}$)	R
Symmetric	2.5 ± 2.5	$95.2\%^{+0.2\%}_{-0.62\%}$
Asymmetric	23 ± 1	98.8% ± 0.14%

(typically ≈ 10 *nm*) eventually limits the bandwidth across which modes are phase locked for sustaining pulse generation.

Thanks to slow light, the cavity length can be drastically reduced compared to classic strip-waveguide-based resonators. For instance, Vujicic *et al.*[1] observed mode-locking with 16 modes within a 10.4 *nm* (1.32 *THz*) bandwidth in a 550 μm long cavity. A PhC cavity similarly exhibiting 16 modes distributed across an 11.5nm band would be around 56 μm long using the n_g = 28 design presented above. The same pulsed signal characteristics could therefore be achieved in a device benefiting from a size reduction that is roughly given by the ratio of the group indices associated with each structure (Table I), i.e. around 8.5 in this case. Depending on the application, the other PhC cavity designs yielding different values of n_g could be used so as to provide either shorter pulse duration (low n_g design) or further miniaturization (high n_g design). The use of modest ng values (<40) makes our approach realistic through providing an increase of the effective cavity length without compromising the optical losses.[30,31]

Finally, we reemphasize that this PhC cavity design is part of a realistic architecture that envisions the combination of several components, each of which has already been demonstrated separately. Regarding the gain medium, we intend to exploit self-assembled InAs/InP quantum dashes[32] vertically embedded in the center of the InP slab, as already used in PhC lasers[32] or waveguide based mode-locked lasers.[1,9,11] The spectral gain of such an active medium is much wider than the bandwidth (≈10 *nm*) of our intended mode-locked laser, so that the gain dispersion should not alter the frequency equidistant comb of modes. Regarding the saturable absorber, graphene is an ideal candidate thanks to its good saturable absorption properties as well as its 2D geometry which leans itself towards integration on planar structures.[33] Successful demonstrations of graphene transferred on both passive[34] or active PhC cavities[33] have been reported in the literature, while evanescent field interaction with graphene has already been used as saturable absorption mechanism in fiber mode-locked lasers.[35] The related effective index change of the guided mode in the presence of graphene should be less than 1.5%, while the selective patterning of graphene should allow us to roughly locate the absorption section near the PhC mirrors, so as to minimize the effect of parasitic reflections due to the effective index change of the guided mode. Although the demonstration of a mode-locked PhC laser under optical pumping would be a significant step forward, we stress that electrical pumping schemes have been demonstrated with PhC lasers.[21,22,36,37] The prevalent approach involving a lateral p-i-n junction,[21,22,36] in particular, could be adapted to our structure. In summary, our cavity design could be readily combined with all the components necessary to laser mode-locking operation (saturable absorber, gain medium), while its its robust geometry (InP/SiO_2, modest n_g) makes it practical for the realization of integrated mode-locked PhC lasers.

IV. CONCLUSION

We designed compact (<100 μm) InP based micro-cavities by exploiting slow light modes in planar PhC geometries for the miniaturization of near-infrared integrated mode-locked lasers. Thanks to dispersion engineering, we managed to tailor the mode dispersion of our PhC structures such that it exhibits both a high and relatively constant group index across a substantial bandwidth, all being prerequisites to mode-locking operation in short cavities. Simulations showed that a 30 μm long cavity based on an optimized PhC design with a group index n_g = 28 can exhibit at least 9 equally-spaced modes with a *FSR* of 178 *GHz* spread across a bandwidth over 11.5 *nm*, potentially affording the generation of ultrashort optical pulses (<700*fs*). Moreover, despite the loss penalty associated with our asymmetric vertical configuration, the quality factors of these modes were all greater than 10, 000, which should be sufficient for enabling laser operation. Most importantly, slow light modes provide a reduction of the cavity length by almost an order of magnitude as compared with more standard rib-waveguide geometries; while achieving similar performance. This shows that the slow light approach can relax the traditional constraint that tightly links the pulsed signal quality and the laser device size. Finally, despite the additional constraints associated with the InP on silica heterostructure used in our study, the practical configuration of our designed cavity allows a saturable absorber to be transferred on top of the structure, while being robust and conducive to integration with a silicon photonic circuit.

ACKNOWLEDGMENTS

The authors acknowledge the support of the ERC project GRAPHICS (consolidator grant n^o 648546) funded under the H2020 European framework.

[1] V. Vujicic, C. Calò, R. Watts, F. Lelarge, C. Browning, K. Merghem, A. Martinez, A. Ramdane, and L. P. Barry, "Quantum dash mode-locked lasers for data centre applications," IEEE Journal of Selected Topics in Quantum Electronics **21**, 53–60 (2015).
[2] J. Luo, N. Calabretta, J. Parra-Cetina, S. Latkowski, R. Maldonado-Basilio, P. Landais, and H. J. S. Dorren, "320 Gb/s all-optical clock recovery and time de-multiplexing after transmission enabled by single quantum dash mode-locked laser," Optics Letters **38**, 4805–8 (2013).
[3] R. Salem, M. A. Foster, A. C. Turner-Foster, D. F. Geraghty, M. Lipson, and A. L. Gaeta, "High-speed optical sampling using a silicon-chip temporal magnifier," Optics Express **17**, 4324–4329 (2009).
[4] C. Mesaritakis, A. Kapsalis, A. Bogris, D. Syvridis, and K. J. Vahala, "Artificial neuron based on integrated semiconductor quantum dot mode-locked lasers," Scientific Reports **6**, 39317 (2016).
[5] V. Moskalenko, J. Koelemeij, K. Williams, and E. Bente, "Study of extra wide coherent optical combs generated by a QW-based integrated passively mode-locked ring laser," Optics Letters **42**, 1428 (2017).
[6] M.-C. Lo, R. Guzmán, M. Ali, R. Santos, L. Augustin, and G. Carpintero, "18-THz-wide optical frequency comb emitted from monolithic passively mode-locked semiconductor quantum-well laser," Optics Letters **42**, 3872 (2017).
[7] J. H. Marsh and L. Hou, "Mode-locked laser diodes and their monolithic integration," IEEE Journal of Selected Topics in Quantum Electronics **23**, 1–11 (2017).
[8] R. Guzmán, C. Gordon, L. Orbe, and G. Carpintero, "1 GHz InP on-chip monolithic extended cavity colliding-pulse mode-locked laser," Optics Letters **42**, 2318 (2017).
[9] S. Joshi, C. Calò, N. Chimot, M. Radziunas, R. Arkhipov, S. Barbet, A. Accard, A. Ramdane, and F. Lelarge, "Quantum dash based single section mode locked lasers for photonic integrated circuits," Optics Express **22**, 11254 (2014).
[10] S. Latkowski, V. Moskalenko, S. Tahvili, L. Augustin, M. Smit, K. Williams, and E. Bente, "Monolithically integrated 25 GHz extended cavity mode-locked ring laser with intracavity phase modulators," Optics Letters **40**, 77 (2015).
[11] K. Merghem, A. Akrout, A. Martinez, G. Aubin, A. Ramdane, F. Lelarge, and G. H. Duan, "Pulse generation at 346 GHz using a passively mode locked quantum-dash-based laser at 1.55 μm," Applied Physics Letters **94**, 1–4 (2009).
[12] T. Thiessen and J. K. S. Poon, "20 GHz Mode-locked laser diodes with integrated optical feedback cavities in a generic monolithic InP photonics platform," IEEE Photonics Journal **9**, 1–10 (2017).
[13] A. A. Lagatsky, A. Choudhary, P. Kannan, D. P. Shepherd, W. Sibbett, and C. T. A. Brown, "Fundamentally mode-locked, femtosecond waveguide oscillators with multi-gigahertz repetition frequencies up to 15 GHz," Optics Express **21**, 19608 (2013).
[14] A. Martinez and S. Yamashita, "10 GHz fundamental mode fiber laser using a graphene saturable absorber," Applied Physics Letters **101**, 041118 (2012).
[15] Z. Wang, M. L. Fanto, J. A. Steidle, A. A. Aboketaf, N. A. Rummage, P. M. Thomas, C.-S. Lee, W. Guo, L. F. Lester, and S. F. Preble, "Passively mode-locked InAs quantum dot lasers on a silicon substrate by Pd-GaAs wafer bonding," Applied Physics Letters **110**, 141110 (2017).
[16] J. Van Campenhout, P. Rojo Romeo, P. Regreny, C. Seassal, D. Van Thourhout, S. Verstuyft, L. Di Cioccio, J.-M. Fedeli, C. Lagahe, and R. Baets, "Electrically pumped InP-based microdisk lasers integrated with a nanophotonic silicon-on-insulator waveguide circuit," Optics Express **15**, 6744 (2007).
[17] D. Liang, M. Fiorentino, T. Okumura, H.-H. Chang, D. T. Spencer, Y.-H. Kuo, A. W. Fang, D. Dai, R. G. Beausoleil, and J. E. Bowers, "Electrically-pumped compact hybrid silicon microring lasers for optical interconnects," Optics express **17**, 20355–64 (2009).
[18] J. Zhang, Y. Li, S. Dhoore, G. Morthier, and G. Roelkens, "Unidirectional, widely-tunable and narrow-linewidth heterogeneously integrated III-V-on-silicon laser," Optics Express **25**, 7092 (2017).
[19] T. J. Karle, Y. Halioua, F. Raineri, P. Monnier, R. Braive, L. Le Gratiet, G. Beaudoin, I. Sagnes, G. Roelkens, F. van Laere, D. Van Thourhout, and R. Raj, "Heterogeneous integration and precise alignment of InP-based photonic crystal lasers to complementary metal-oxide semiconductor fabricated silicon-on-insulator wire waveguides," Journal of Applied Physics **107**, 063103 (2010).
[20] Y. Halioua, A. Bazin, P. Monnier, T. J. Karle, G. Roelkens, I. Sagnes, R. Raj, and F. Raineri, "Hybrid III-V semiconductor/silicon nanolaser," Optics Express **19**, 9221 (2011).
[21] K. Takeda, T. Sato, T. Fujii, E. Kuramochi, M. Notomi, K. Hasebe, T. Kakitsuka, and S. Matsuo, "Heterogeneously integrated photonic-crystal lasers on silicon for on/off chip optical interconnects," Optics Express **23**, 702 (2015).
[22] G. Crosnier, D. Sanchez, S. Bouchoule, P. Monnier, G. Beaudoin, I. Sagnes, R. Raj, and F. Raineri, "Hybrid indium phosphide-on-silicon nanolaser diode," Nature Photonics **11**, 297–300 (2017).
[23] K. Takeda, T. Sato, A. Shinya, K. Nozaki, W. Kobayashi, H. Taniyama, M. Notomi, K. Hasebe, T. Kakitsuka, and S. Matsuo, "Few-fJ/bit data transmissions using directly modulated lambda-scale embedded active region photonic-crystal lasers," Nature Photonics **7**, 569–575 (2013).
[24] Y. Liu, Z. Wang, M. Han, S. Fan, and R. Dutton, "Mode-locking of monolithic laser diodes incorporating coupled-resonator optical waveguides," Optics Express **13**, 4539 (2005).
[25] C. Monat, C. Seassal, X. Letartre, P. Regreny, M. Gendry, P. Rojo Romeo, P. Viktorovitch, M. Le Vassor D'yerville, D. Cassagne, J. P. Albert, E. Jalaguier, S. Pocas, and B. Aspar, "Two-dimensional hexagonal-shaped microcavities formed in a two-dimensional photonic crystal on an InP membrane," Journal of Applied Physics **93**, 23–31 (2003).
[26] Y. Tanaka, T. Asano, R. Hatsuta, and S. Noda, "Analysis of a line-defect waveguide on a silicon-on-insulator two-dimensional photonic-crystal slab," Journal of Lightwave Technology **22**, 2787–2792 (2004).

[27] J. Li, T. P. White, L. O'Faolain, A. Gomez-Iglesias, and T. F. Krauss, "Systematic design of flat band slow light in photonic crystal waveguides," Optics Express **16**, 6227–6232 (2008).
[28] B. Corcoran, C. Monat, M. Pelusi, C. Grillet, T. P. White, L. O'Faolain, T. F. Krauss, B. J. Eggleton, and D. J. Moss, "Optical signal processing on a silicon chip at 640Gb/s using slow-light," Optics Express **18**, 7770 (2010).
[29] M. Heuck, S. Blaaberg, and J. Mørk, "Theory of passively mode-locked photonic crystal semiconductor lasers," Optics Express **18**, 18003–18014 (2010).
[30] N. Le Thomas, H. Zhang, J. Jágerská, V. Zabelin, R. Houdré, I. Sagnes, and A. Talneau, "Light transport regimes in slow light photonic crystal waveguides," Physical Review B **80**, 125332 (2009).
[31] L. O'Faolain, S. A. Schulz, D. M. Beggs, T. P. White, M. Spasenović, L. Kuipers, F. Morichetti, A. Melloni, S. Mazoyer, J. P. Hugonin, P. Lalanne, and T. F. Krauss, "Loss engineered slow light waveguides," Optics Express **18**, 27627–27638 (2010).
[32] B. Ben Bakir, C. Seassal, X. Letartre, P. Regreny, M. Gendry, P. Viktorovitch, M. Zussy, L. Di Cioccio, and J.-M. Fedeli, "Room-temperature InAs/InP quantum dots laser operation based on heterogeneous "2.5 D" photonic crystal," Optics Express **14**, 9269 (2006).
[33] M.-S. Hwang, H.-R. Kim, K.-H. Kim, K.-Y. Jeong, J.-S. Park, J.-H. Choi, J.-H. Kang, J. M. Lee, W. I. Park, J.-H. Song, M.-K. Seo, and H.-G. Park, "Switching of photonic crystal lasers by graphene," Nano Letters **17**, 1892–1898 (2017).
[34] T. Gu, N. Petrone, J. F. McMillan, A. van der Zande, M. Yu, G. Q. Lo, D. L. Kwong, J. Hone, and C. W. Wong, "Regenerative oscillation and four-wave mixing in graphene optoelectronics," Nature Photonics **6**, 554–559 (2012).
[35] Y.-W. Song, S.-Y. Jang, W.-S. Han, and M.-K. Bae, "Graphene mode-lockers for fiber lasers functioned with evanescent field interaction," Applied Physics Letters **96**, 051122 (2010).
[36] B. Ellis, M. A. Mayer, G. Shambat, T. Sarmiento, J. Harris, E. E. Haller, and J. Vučković, "Ultralow-threshold electrically pumped quantum-dot photonic-crystal nanocavity laser," Nature Photonics **5**, 297–300 (2011).
[37] H.-G. Park, "Electrically driven single-cell photonic crystal laser," Science **305**, 1444–1447 (2004).